Global Journal of Researches in Engineering: D
Aerospace Science
Volume 21 Issue 1 Version 1.0 Year 2021
Type: Double Blind Peer Reviewed International Research Journal
Publisher: Global Journals
Online ISSN: 2249-4596 & Print ISSN: 0975-5861

Airfoil Analysis and Effect of Wing Shape Optimization on Aerodynamic Parameters in a Steady Flight

By Vishu K. Oza & Hardik R. Vala
Silver Oak University

Abstract- The work in this paper deals with reconstructing and optimizing the wing geometry of an Unmanned Combat Aerial Vehicle for improved performance and reviewing the impact of the modification on flight parameters in a steady flight. The behavior of airfoils at planned flight conditions under I.S.A. is checked in XFLR5 software. Following up by 2-D CFD and boundary layer analysis of former and new airfoil, dimensions of the wing are re-developed, keeping the fuselage and tail structure same. The existing wing and the optimized wing design is analyzed by Vortex Lattice Method and Triangular Panel Method, with an objective to make the shape of the wing aerodynamically suitable for an increased Lift to Drag ratio and thereby minimizing drag coefficients.

Keywords: airfoil, boundary layer, CFD, wing, optimization, (L/D).

GJRE-D Classification: FOR Code: 290201

AIRFOILANALYSISANDEFFECTOFWINGSHAPEOPTIMIZATIONONAERODYNAMICPARAMETERSINASTEADYFLIGHT

Strictly as per the compliance and regulations of:

Airfoil Analysis and Effect of Wing Shape Optimization on Aerodynamic Parameters in a Steady Flight

Vishu K. Oza [α] & Hardik R. Vala [σ]

Abstract- The work in this paper deals with reconstructing and optimizing the wing geometry of an Unmanned Combat Aerial Vehicle for improved performance and reviewing the impact of the modification on flight parameters in a steady flight. The behavior of airfoils at planned flight conditions under I.S.A. is checked in XFLR5 software. Following up by 2-D CFD and boundary layer analysis of former and new airfoil, dimensions of the wing are re-developed, keeping the fuselage and tail structure same. The existing wing and the optimized wing design is analyzed by Vortex Lattice Method and Triangular Panel Method, with an objective to make the shape of the wing aerodynamically suitable for an increased Lift to Drag ratio and thereby minimizing drag coefficients.

Keywords: *airfoil, boundary layer, CFD, wing, optimization, (L/D).*

I. Introduction

The aerodynamic performance of an aerial vehicle is governed by ample factors, including the main components of aircraft; however, the wing is a primary unit for driving performance in a favorable direction. The wing design should be such that it should be preferable for desired lift production at a given altitude. 'Drag' is a key aerodynamic parameter to be considered, and so it should be as minimum as possible to retain the flight condition and to keep the flow environment undisturbed. The Lift to Drag (L/D) ratio of an aircraft signifies how efficient the design of an aircraft is and which will tend to deliver lift at low drag with better performance.

The intention here is to elevate the (L/D) ratio of an aircraft at the expense of the wing's makeover and thereby re-framing the module's geometry. For this purpose, a UCAV model of General Atomics MQ-1B Predator is chosen [1].

Table 1: MQ-1B Predator specifications

W	1020 kg (10006.2 N)
b	16.84 m
c_r	1.0972 m
c_t	0.396 m
λ (c_t/c_r)	0.360 m
MAC	0.801 m
S_{ref}	11.75 m^2
AR	23.63
Λ_{LE}	2 degrees
h	7620 m

The root section of the wing has Drela GW 19 airfoil, and the tip section has GW 27 airfoil developed by Professor Mark Drela from MIT. Airfoil GW 19 [2] and GW 27 [2] have a highly cambered upper surface for lift generation at high velocities in the subsonic regions.

The wing's performance is examined at an altitude of 3000m under the International Standard atmosphere (I.S.A.) [3], where temperature, pressure, and density are T = 268.7 K, p = 70.1 kPa, and ρ = 0.909 kg/m^3, respectively. With kinematic viscosity of v = 1.95x10^{-5} m^2/s, and assuming cruise velocity of 45 m/s and by MAC of 0.801 m, gives Reynolds Number of 1671678 (means turbulent flow nature). With speed of sound at 3000 m, a = 328.6 m/s, Mach number is M = 0.136.

a) 2-D Airfoil analysis

The aerodynamic behavior of all airfoils is analyzed in XFLR5 software, which uses preinstalled codes of XFOIL. Ibrahim Halil Guzelbey et al.[4], their paper of 2018 deals with comparing experimental wind tunnel data with XFLR5's generated one for airfoils. The work of Popelka Lukas et al [5]. shows behavior of various airfoils for a sailplane studied in XFLR5 software. Additionally, the flow transition prediction on a 3D wing was also made using the same software. In the present paper, 2-D airfoil analysis has been performed to determine the nature of GW 19, GW 27, and NACA 2315 (it is modified from the conventional NACA 2412 airfoil, by changing the position of its maximum camber and maximum thickness [6]) airfoils from -10 to 30-degree angle of attack (α) at proposed flight condition. From Figure 1. of generated polar, it is clear that the lift coefficient of NACA 2315 is quite less in a low range of angles while drag coefficient is moderately lesser than

Author α: Student, Department of Mechanical Engineering, Silver Oak University, Gujarat, India. e-mail: ozavshu@gmail.com
Author σ: Assistant Professor, Department of Aeronautical Engineering, Silver Oak University, Gujarat, India. e-mail: hardikvala.ae@socet.edu.in

both GW airfoils. From graph polar for GW19, Cl_{max} is 1.762 at 20 degrees. While a sharp stall after 16 degrees is seen for the new NACA 2315 airfoil, giving out Cl_{max} of 1.563. So, the estimated stall velocity is 34.26 m/s.

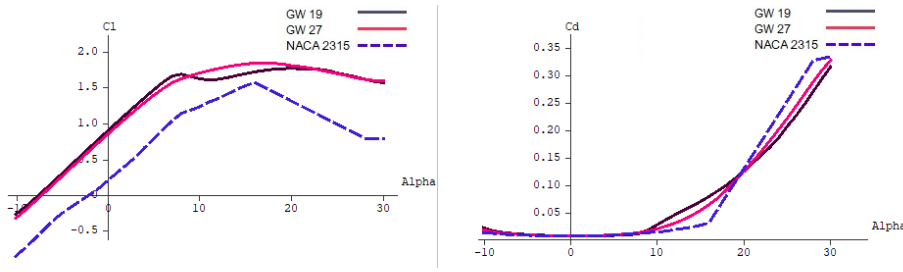

Figure 1: Comparison of Lift and Drag coefficients for airfoils

Furthermore, 2D steady flow analysis has been done in StarCCM+ software, which sets Reynolds Averaged Navier Stokes (RANS) equations, which are used to define turbulent flow by giving approximate solutions. Manuel J. Garcia, Pierre Boulanger, and Santiago Giraldo [7] have worked on aerodynamic profiles optimized with gradient methods. Additionally, the k-epsilon model of turbulence, with Navier Stokes equations, is used for CFD simulations. Jörg Schminder [8], in his thesis, imposed RANS for the computational study of hornet aircraft. To note that, for the shear stress model, k-epsilon was used as k-omega is more sensible to streamlined flow. From the work of Junling Hu, Xingguo Xiong, and Linfeng Zhang, it was seen that the Spalart Allmaras model was not used because of the airfoil's highly cambered surface [9]. Lucas Popelka et al. [10], suitability of the k-epsilon model is well underlined as the flow involves rotation and adverse pressure gradients in a boundary layer. To acknowledge the flow fields, which are shown in Figure 2. And Figure 3, 11131 cells were created by defining the wake refinement length of 3.5 m.

Table 2: Physical model assignation for CFD analysis

Fluid type	Gas
Flow type	Segregated flow
Viscous regime	Turbulent
Shear Stress Transport model	k - epsilon turbulence
Reference pressure	70.10 kPa
Reference velocity	45 m/s
Reference density	0.909 kg/m^3
Domain inlet	Velocity inlet
Domain outlet	Pressure outlet

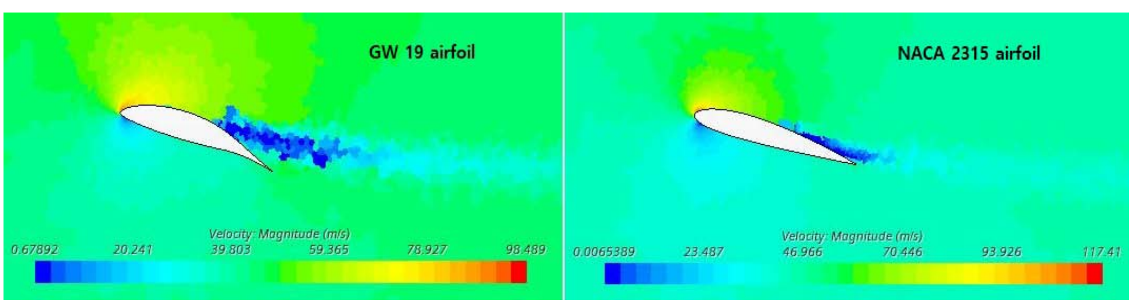

Figure 2: Velocity field at stall angles

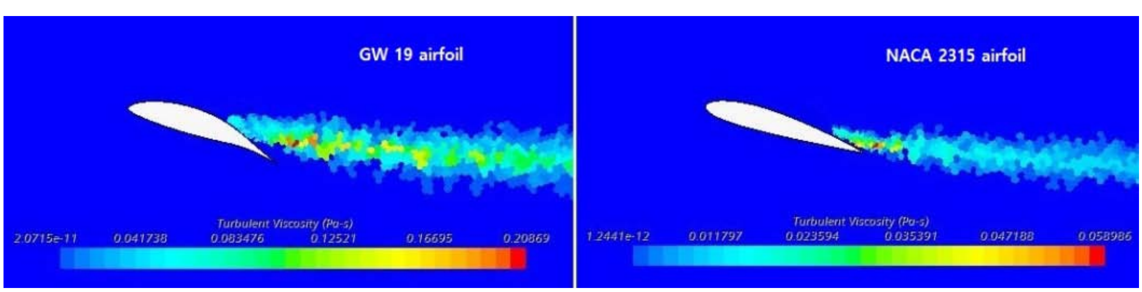

Figure 3: Turbulent viscosity at stall angles

Figure 2 and Figure 3 depict the flow separation phenomena over the airfoils at their respective stall angles. At some point, when flow separates (making velocity negative) on an airfoil, inside a formed bubble, the flow goes turbulent, progressing further, flow again reattaches, making velocity positive and leaving the trailing edge wakes.

Consider a small elemental strip of thickness 'dy' at y distance from the surface of a plate, and at a thickness δ, where fluid velocity 'u' (which is a function of x and y direction at any section) is 99 percent of free stream velocity 'u_∞', where δ is Boundary layer thickness.

In a boundary layer problem, the velocity field is used as an input, which does not converge, as boundary layer disturbs the inviscid flow, and airfoil acts as it has an additional thickness δ^*, called "Displacement thickness" [11], which is represented as,

$$\delta^* = \int_0^\delta (1 - \frac{u}{u_\infty})dy \qquad (1)$$

Additionally, a flow layer, for which the momentum flux is equal to the deficit for the same thru boundary layer, is called Momentum thickness θ [11],

$$\theta = \int_0^\delta \frac{u}{u_\infty}\left(1 - \frac{u}{u_\infty}\right)dy \qquad (2)$$

The software uses the Interactive boundary layer solver, having an integral turbulence model created by Professor T. Cebeci [12].

Assumptions for boundary layer analysis are,

1. Sharp velocity gradients are smoothed at trailing edge from inviscid analysis before boundary layer analysis as fluid nature at trailing edge is not reliably predicted by inviscid analysis due to Kutta condition [11].
2. Turbulence is forced at separation, as the transition is always induced by it.

The variation of $\delta^*$and θ with chord length (X) of 1 m is shown in Figure 4. for GW19 and NACA 2315, at planned condition.

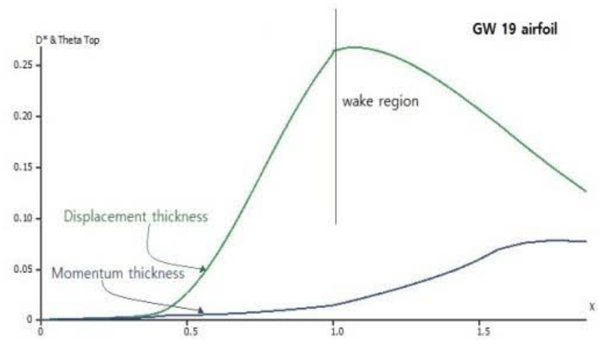

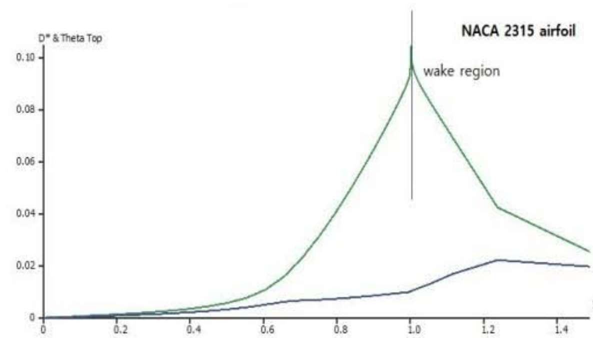

Figure 4: Variation in Displacement and Momentum thickness

From Interactive boundary layer analysis, the top flow transition for GW 19 and NACA 2315 airfoil is predicted as

Table 3: For GW 19 airfoil

Flow nature	chord location(m)
Laminar to turbulent	0.645
Laminar separation	0.645
Turbulent separation	0.656

Table 4: For NACA 2315 airfoil

Flow nature	chord location(m)
Laminar to turbulent	0.487
Laminar separation	0.487
Turbulent separation	1.04

From values in Table 3., and Table 4., it is seen that flow is getting turbulent on GW 19's top surface at 0.64 m of length and wakes are formed at 0.656 after turbulent flow separation. However, the transition is a little ahead in NACA 2315's top surface, and turbulent flow is separated at 1.04 m of the chord length, which means the boundary layer is maintained on the top surface.

The software uses the e^N method for boundary layer transition prediction, which is a free transition method, where the N_{crit} value has to be defined for flow's changeover. The e^N, with an amplification factor (N), operates as growing Tollmien-Schlichting waves, J.L van Ingen [13]. For an average experimental wind tunnel, the default N_{crit} is 9, which is pre-setted in XFLR5 from 2-D boundary layer analysis. Again, as seen in the airfoil's coefficient of pressure (C_p) plot and plot of edge velocity against chord length, the laminar separation for GW 19 is before the NACA 2315 airfoil, as seen in Figure 5. and Figure 6. respectively.

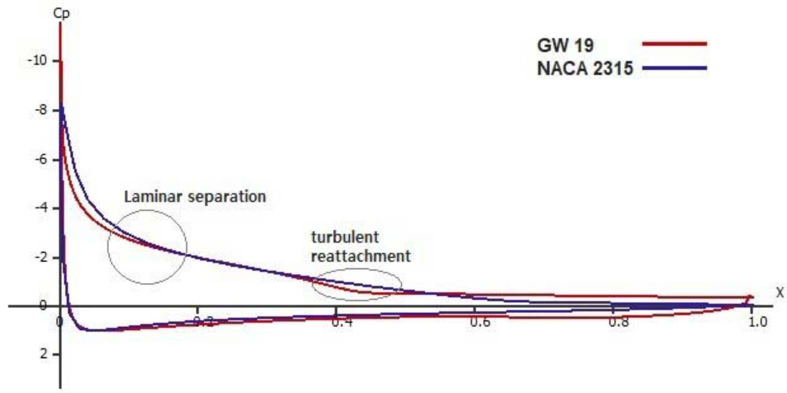

Figure 5: Variation in pressure coefficients at stall angle

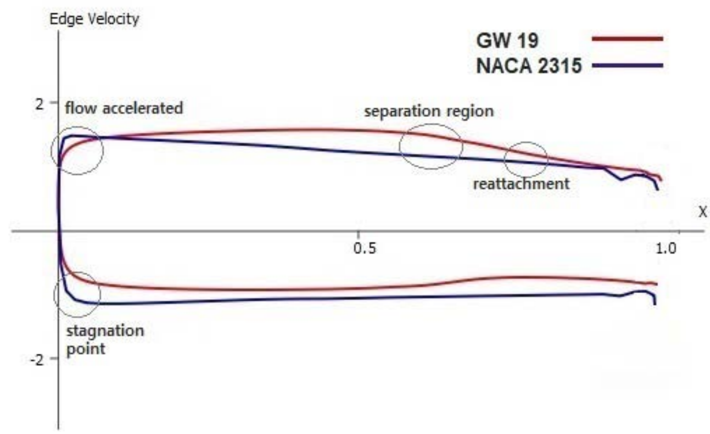

Figure 6: Variation in edge velocity at stall angles

II. Wing Design and Analysis

For new construction with load distribution sectionally, the wing is divided into four sections. For the lower bending moments, the load should concentrate at the root. The configuration has been kept the same as mid-wing. Wing sweep is generally provided in transonic aircraft for delaying the wave drag, it also improves static lateral stability and moderately reduces dynamic pressure, and so is given, M. Sadraey [14].

From the work of Boitumelo Makgantai et al. [15], winglets can be implemented for reducing induced drag and increasing (L/D) ratio.

The wing is not twisted in any of the four sections. For directional stability, dihedral is provided in section three as well as section two. Detailed dimensions of the wing are provided below, having NACA 2315 airfoil at all four sections.

Table 5: Detailed dimensions of the new wing

Wing section	Span position(m)	Chord (m)	Sweepback (degree)	Dihedral (degree)
1	0.385	0.865	3.5	0
2	5.80	0.64	8	7
3	8.50	0.401	35	40
4	10	0.120	0	0

a) *3-D analysis approach*

Starting with Navier Stokes equation, for solving the greater part of the complexity, by assumption of time-dependent incompressible flow, gives out Laplace equation ($\nabla^2\phi = 0$). On computation via time-averaged turbulence, which derives the Reynolds equation, is comprised in RANS solver.

For analysis in XFLR5, the Laplace equation is solved, satisfying the given boundary condition. Boundary conditions taken into account are of Dirichlet or Neumann type. Of mathematical type, the Dirichlet boundary condition specifies the value of a potential function at a specific location. While Neumann boundary condition specifies the value of the gradient of potential function on surface, $\nabla\phi = \overrightarrow{V_0}$ (which is a velocity vector). XFLR5 interpolates viscous results from XFOIL and reintroduces them in the 3-D inviscid solution.

Vortex Lattice Method (VLM), having many vortices in panels, is fitted with Neumann boundary condition. The approach to this method comprises of one ring vortex present on each meshed region on a point. VLM models the disturbance formed on a wing, by summation of vortices, and the strength of a single vortex is examined by an imposed boundary condition. VLM is selected for current analysis because the flow is considered inviscid and potential, Chethan R. Patil et al. [16], and additionally only induced drag can be measured, A. Septiyana et al. [17]. Oliviu Sugar Gabor et al. [18] preferred XFLR5 to compare the aerodynamic characteristics of a wing with the non-linear VLM method and experimental's. Even it can be used for stall prediction, Hasier Goitia, Raúl Llamas [19].

Cian Conlan-Smith et al. [20] have implemented panel methods for wing's analytical study and it is stated that the use of quad panels is not preferable because just three points are taken for plane definition as the quad panel may not cover a 3-D curved surface completely. In the Triangular panel method, each quad panel is replaced by two triangles of uniform density. Then, the wing surface can be treated as a thin sheet, and this method involves solving meshed triangular surface integrals on it, along with the defined boundary condition.

Before the wing's analysis in XFLR5, Parasite Drag acting on the wetted area is taken into account, using OpenVSP software. The flow solver in OpenVSP is based on VLM, Ilias Lappas, and Akira Ikenaga [21]. The usage of OpenVSP software for computing aircraft Cessna's model is noted in work by Marine Segui and Ruxandra Mihaela Botez [22]. Andrew S. Hahn [23] had depicted the suitability of the OpenVSP software for complex parameterized geometries like fuselage and fairings. Additionally, any kind of complex wing geometry, having multi-sections with different airfoils, can be easily modeled in OpenVSP, William J. Fredericks [24].

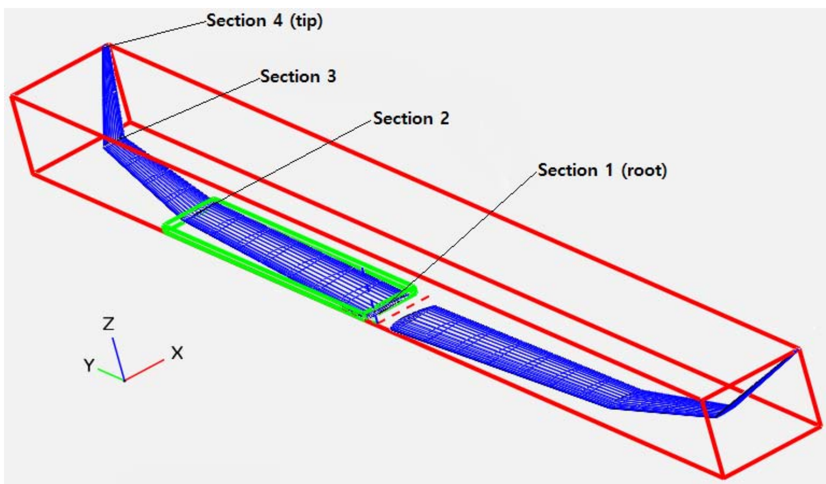

Figure 7: CAD model of new wing created in OpenVSP

The viscous drag coefficient is difficult to predict by numerical methods and is based on experimental data and is generally taken 0.005 for vehicles flying at Reynolds number more than 200000. Here, the surface roughness of the upper surface of the wing is assumed to be uniform.

For calculating, net viscous drag coefficient on net wetted area, equations selected for skin friction coefficients [25] are,

1. Laminar skin friction coefficient: Blasius equation

$$C_f = \frac{1.32824}{\sqrt{Re}} = 0.00102 \tag{3}$$

2. Turbulent skin friction coefficient: Power Law High Reynolds Number

$$C_f = \frac{0.0725}{Re^{(1/5)}} = 0.00412 \tag{4}$$

Ohad Gur et al.[26], for estimating skin friction drag, Torenbeek's and Hoerner's equation for Form Factor (FF) have been taken into consideration, as both are the function of airfoil's thickness to chord (t/c) ratio.

Form Factor (FF) equation: Average (t/c) for NACA 2315 is 0.14009, so with the Hoerner equation,

$$FF = 1 + 2\left(\frac{t}{c}\right) + 60\left(\frac{t}{c}\right)^4 = 1.33 \tag{5}$$

The reference area for the new wing is $S_{ref} = 11.75\ m^2$, wetted area $S_{wet} = 24.24\ m^2$ and $C_{Do} = 0.01118$, Equivalent viscous drag coefficient can be calculated following equation [26],

$$C_{fe} = FF \times C_{Do} \times \left(\frac{S_{ref}}{S_{wet}}\right) = 0.0071 \tag{6}$$

The value of C_{fe}, if FF is not taken into consideration, is near to one of the single-engine light aircraft (0.0055), as seen in the work by Abderrahmane Badis[27]. With $\mathrm{AR} = 34$, XFLR5's (by VLM) generated $C_L = 0.54$, induced drag coefficient $C_{Di} = 0.0054$, and assuming the span efficiency e = 0.5, the total drag coefficient is given as [28],

$$C_D = C_{Do} + \left(\frac{C_L{}^2}{\pi\ AR\ e}\right) = 0.0165 \tag{7}$$

So, Lift to Drag ratio (L/D) = (C_L/C_D) = 32.7.

III. Wing Optimization

Optimization is either minimizing or maximizing the objective function. Here Covariance Matrix Adaptation Evolution Strategy (CMA-ES) is implemented for the intended purpose. It involves generating the finite solutions, then evaluating them and selecting accurate one of them, and reproducing the next set of finite solutions until iterations are terminated. The solution which is generated optimum from both sets of iterations is considered as an optimum solution. In the thesis work of Matthieu Parenteau [29], the design variables are manipulated for better performance requirements, by using the CMA-ES algorithm.

Wing shape optimization

Objective function = Maximize: (L/D)

Maximize: f = $L/D(x)$; $i = 1$ to 100

Total design variables = 12

Table 6: Selected design variables

Sr. No	Design Variable	Base value	Lower bound	Upper bound	Units
1	Span position (1st section)	0.385	0.32	0.42	m
2	Span position (2nd section)	5.8	5.4	6	m
3	Span position (3rd section)	8.5	8.3	8.7	m
4	Span position (4th section)	10	9.7	10.3	m
5	Chord (1st section)	0.860	0.8	0.9	m
6	Chord (2nd section)	0.64	0.5	0.7	m
7	Chord (3rd section)	0.401	0.3	0.5	m
8	Chord (4th section)	0.12	0.1	0.4	m
9	Sweepback (1st section)	3.5	2	4	degree
10	Sweepback (2nd section)	8	6	10	degree
11	Dihedral (2nd section)	7	6.8	9	degree
12	Dihedral (3rd section)	40	39	41	degree

Table 7: Optimum dimensions after 100 iterations

Wing section	Span position(m)	Chord (m)	Sweepback (degree)	Dihedral (degree)
1	0.355	0.8	4	0
2	5.903	0.546	8.366	6.8
3	8.602	0.388	35	40.757
4	10.202	0.1	0	0

The optimized NACA 2315 wing is analyzed at the same flight condition at α = 2.5 degrees, with wingspan $b = 20.4\ \mathrm{m}$, $S_{ref} = 10.77\ \mathrm{m}^2$, and $\mathrm{AR} = 38.64$. Higher the AR, lower will be the induced drag (coefficient). Again, the parasite drag coefficient is calculated in OpenVSP by following the same steps. With wetted area $S_{wet} = 22.21\ \mathrm{m}^2$, the parasite drag coefficient acting is $C_{Do} = 0.01143$.

Following is the detailed analysis for an initial wing and optimized wing, done by both VLM and Panel methods.

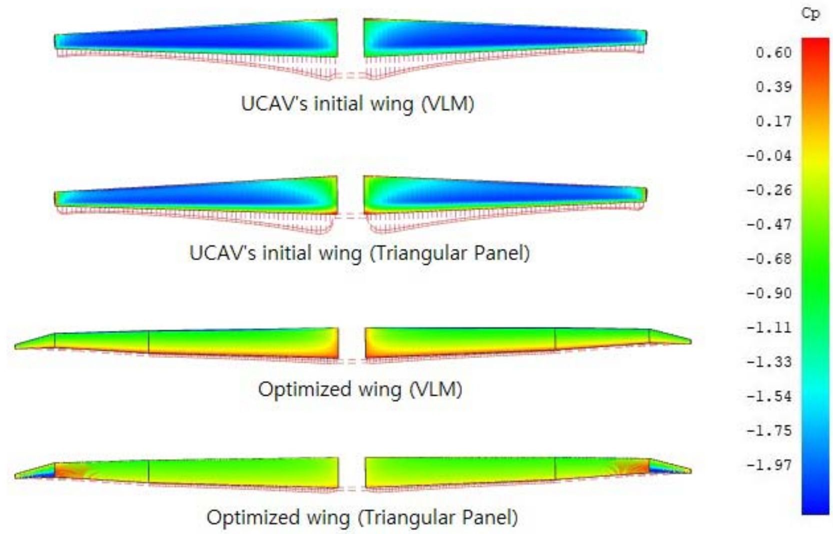

Figure 8: Variation in pressure distribution on the upper surface of the initial wing and optimized wing by both methods

Table 8: Aerodynamic coefficients for initial wing

Method	C_L	C_{Di}	C_{Do}	C_D	C_{fe}	(C_L/C_D)
VLM (Neumann)	0.600	0.0097	0.0119	0.0216	0.0072	27.77
Panel (Dirichlet)	0.612	0.010	0.0119	0.0219	0.0072	27.94

Table 9: Aerodynamic coefficients for optimized wing

Method	C_L	C_{Di}	C_{Do}	C_D	C_{fe}	(C_L/C_D)
VLM (Neumann)	0.55	0.0049	0.0114	0.0163	0.0071	33.74
Panel (Dirichlet)	0.581	0.0055	0.0114	0.0169	0.0071	34.37

IV. Results and Discussion

From Figure 9 It can be seen that the initial wing has elliptical lift distribution, not completely, due to span efficiency is less than 1. The maximum C_L is at the midspan and drastically decreases approaching the tip, as vortices are formed. While, for the optimized wing, the distribution remains near-uniform from mid-span and at tip section, it is maintained as induced drag is minimized. Also, from the results by VLM analysis, C_L is little more than at tip section, like that of the Triangular panel method analysis.

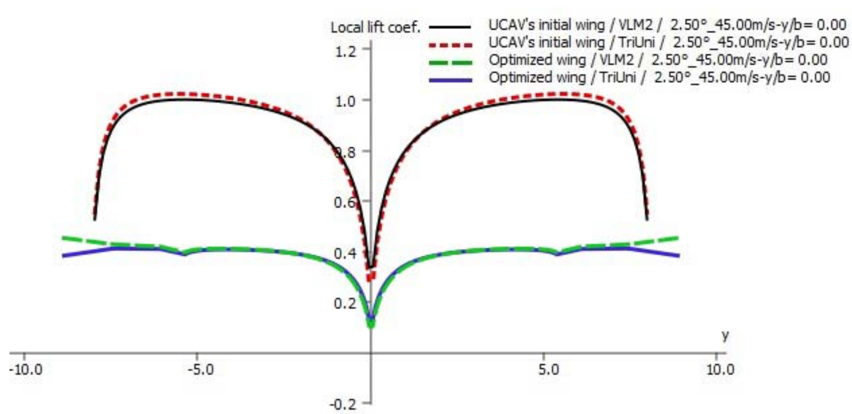

Figure 9: Lift distribution along the wingspan

From Figure 10, the total drag acting at the wing-fuselage section, is substantially decreased for the optimized wing design. By analysis of the VLM method, for the initial wing, the total drag coefficient, comprised of induced drag coefficient, is more at the wing tip section. Induced drag, being a function to total drag, is very much minimized because of near approximate constant elliptical lift distribution in optimized wing design [30] (but indeed not necessary to have provided a twist in airfoil or wing geometry), as seen in Figure 9. However, the total drag coefficient is maintained low over the entire wingspan, and near tip section, by installing winglets, total C_D has highly reduced.

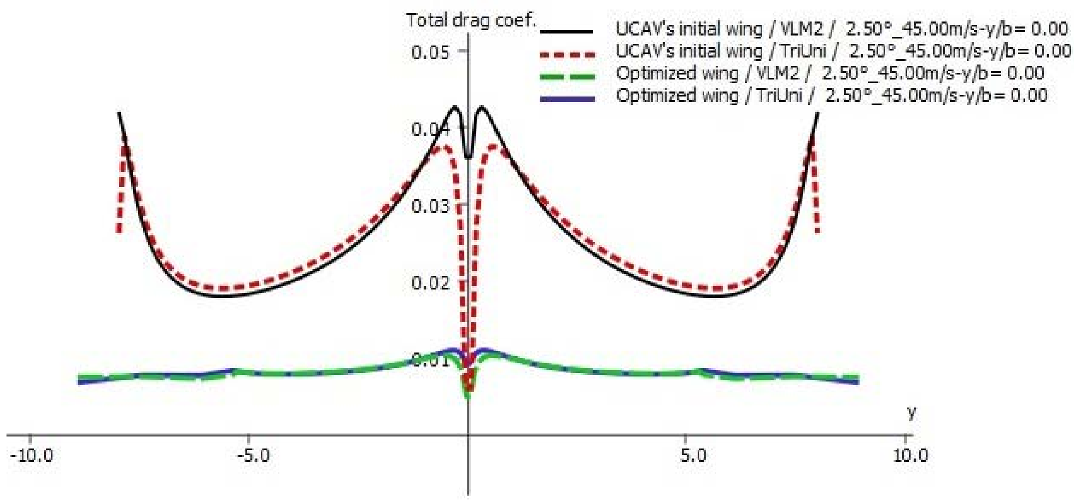

Figure 10: Variation in total drag coefficient along the span

The intention of dividing optimized wing into sections is seen in Figure 11, as the Bending moment of the final wing at the root section, following towards the tip section, is observed as being minimized. Because of the dihedral provided, at sections two as well as three, the Bending moment had gradually decreased from root to tip section as compared to the analysis of the initial wing.

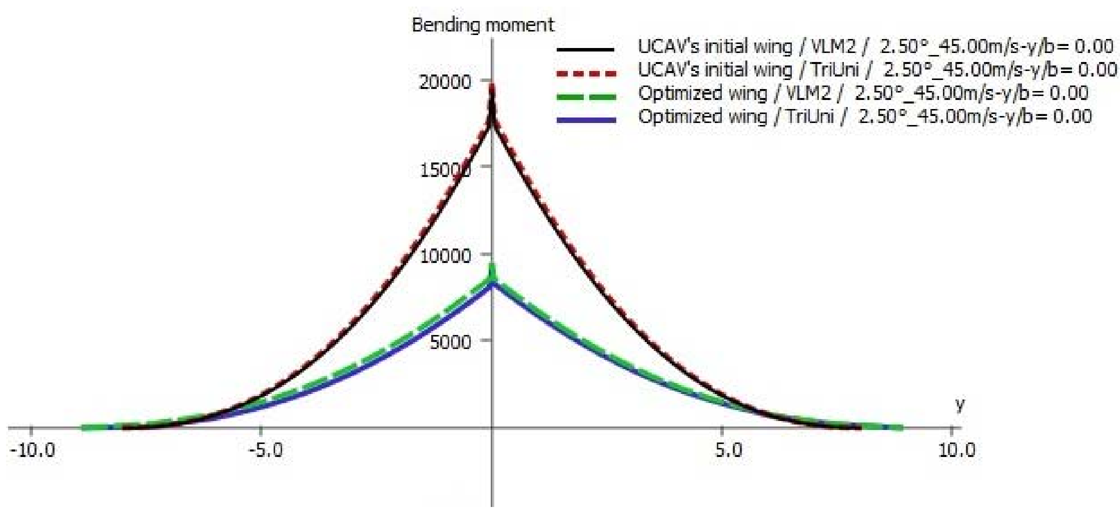

Figure 11: Variation in Bending moment along the wingspan

The airfoil used in the new wing design, for which the boundary layer analysis was done, had delayed the boundary layer separation on the top surface. For 3D wing analysis, the percentage flow transition to turbulent flow for the new wing is less than that of the initial wing. Additionally, moving towards the tip section, as seen in Figure 12, the flow curve is linear as the majority of the vortex shedding had lowered due to the use of winglets.

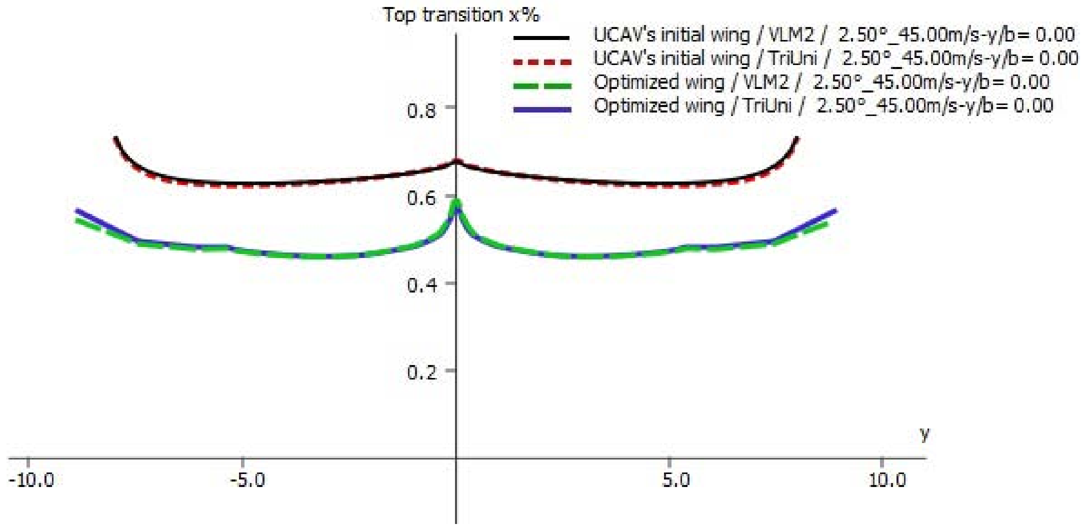

Figure 12: Variation in top flow transition

On the other side, once the C_L and C_D at any particular velocity are obtained, then the product of that velocity and Required Thrust will help in determining the Power required P_{req} as [28],

$$P_{req} = T_{req} \times v = \frac{W}{(\frac{C_L}{C_D})} \times \sqrt{\frac{2W}{\rho \times S_{ref} \times C_L}}$$
$$\text{So, } P_{req} = \sqrt{\frac{2 \times W^3 \times C_D^2}{\rho \times S_{ref} \times C_L^3}} \text{ kW} \quad (8)$$

Considering the UCAV's gross weight constant, at 2.5 degrees, the P_{req} with UCAV's initial wing (by considering the analysis of VLM) comes out to be 19.9 kW, and considering the same method, the optimized wing is 18 kW. So, with an increase in (L/D) ratio, as the total lift and drag coefficients are impacted, about 1.9 kW of power is saved with optimized wing design, and that is economical [31].

V. Conclusion

To elevate the (L/D) ratio of a UCAV, prominent attention has to be given to the design of an airfoil, as its curve is the driving element for desirable flow conditions. In the present work, the airfoil performance of NACA 2315 airfoil, which was designed by modifying the parameters from conventional NACA 2412 airfoil, had proven effective. The Drela GW 19 and GW 27, being high Reynolds Number airfoils, are originally implemented in UCAV MQ-1B Predator's wing design. However, NACA 2315 airfoil can also be used in medium-speed subsonic flight.

For 3-D wing performance, some factors accounted for the steady flight, had proven efficient. Again, the Aspect ratio, which was increased, and the provision of winglets, were two of the weighted governing parameters for reducing the induced and total drag. The optimization results came out to be advantageous, as it did not only reduced total drag but also lowered the wing bending moment and made the wing structurally better.

For future work, how the internal deformation occurs by changing the wing's external topology can be examined so the ribs and spars arrangement can be revised again with a viewpoint of the wing's weight reduction. Furthermore, a complete stability analysis can be performed by introducing the horizontal and vertical stabilizers and their components, making the design of the whole UCAV better statically and dynamically stable.

References Références Referencias

1. "MQ-1B Predator," U.S. Air Force. https://www.af.mil/About-Us/Fact-Sheets/Display/Article/104469/mq-1b-predator/.
2. "General atomics Predator A." https://web.mit.edu/drela/Public/web/hpa/.
3. "International Standard Atmosphere." https://www.engineeringtoolbox.com/international-standard-atmosphere-d_985.html.
4. I. Guzelbey, Y. Eraslan, and M. Doğru, "Numerical Investigation of Different Airfoils at Low Reynolds Number in terms of Aerodynamic Performance of Sailplanes by using XFLR5," vol. 8(1), pp. 47–65, Jun. 2018, doi: 10.31466/kfbd.423932.
5. L. Popelka, M. Matejka, D. Simurda, and N. Souckova, "Boundary Layer Transition, Separation and Flow Control on Airfoils, Wings and Bodies in

Numerical, Wind-Tunnel and In-Flight Studies," Technical Soaring, vol. 35, no. 4, Art. no. 4, Sep. 2011.
6. "NACA 4 digit airfoil generator (NACA 2315 AIRFOIL)." http://airfoiltools.com/airfoil/naca4digit.
7. M. J. Garcia, P. Boulanger, and S. Giraldo, "CFD Based Wing Shape Optimization Through Gradient-Based Method," undefined, 2008, Accessed: Aug. 24, 2021. [Online]. Available: https://www.semanticscholar.org/paper/CFD-Based-Wing-Shape-Optimization-Through-Method-Garcia-Boulanger/bfedeacb625291f219e8a683da8e513ddf893887.
8. J. Schminder, "Feasibility study of different methods for the use in aircraft conceptual design," p. 87.
9. K. Ren, J. Hu, X. Xiong, L. Zhang, and J. Wei, "Validation of Turbulence Models in STAR-CCM+ by N.A.C.A. 23012 Airfoil Characteristics," Apr. 2009.
10. L. Popelka, J. Kuklova, D. Simurda, N. Souckova, M. Matejka, and V. Uruba, "Visuali-zation of boundary layer separation and passive flow control on airfoils and bodies in wind-tunnel and in-flight experiments," EPJ Web of Conferences, vol. 25, p. 01078, 2012, doi: 10.1051/epjconf/20122501078.
11. E. L. Houghton, Ed., Aerodynamics for engineering students, 6th ed. Waltham, MA: Butterworth-Heinemann, 2012.
12. T. Cebeci and J. Cousteix, Modeling and Computation of Boundary-Layer Flows: Laminar, Turbulent and Transitional Boundary Layers in Incompressible and Compress-ible Flows, 2nd ed. Berlin Heidelberg: Springer-Verlag, 2005. doi: 10.1007/3-540-27624-6.
13. J. van Ingen, "The eN Method for Transition Prediction. Historical Review of Work at TU Delft," in 38th Fluid Dynamics Conference and Exhibit, American Institute of Aero-nautics and Astronautics, 2008. doi: 10.2514/6.2008-3830.
14. M. Sadraey and D. W. College, "CHAPTER 5 WING DESIGN," p. 109.
15. B. Makgantai, N. Subaschandar, and R. S. Jamisola, "Design Optimization of Wingtip Devices to Reduce Induced Drag on Fixed-Wings," in 2021 International Conference on Unmanned Aircraft Systems (ICUAS), Jun. 2021, pp. 1459–1465. doi: 10.1109/ICUAS51884.2021.9476801.
16. K. K. Chaitanyaa, C. R. Patil, B. Pal, and D. Dandotiya, "Aerodynamic Analysis and Optimization of Airfoils Using Vortex Lattice Method," IOP Conf. Ser.: Mater. Sci. Eng., vol. 1013, p. 012023, Jan. 2021, doi: 10.1088/1757-899X/1013/1/012023.
17. A. Septiyana et al., "Analysis of aerodynamic characteristics using the vortex lattice method on twin tail boom unmanned aircraft," AIP Conference Proceedings, vol. 2226, no. 1, p. 020003, Apr. 2020, doi: 10.1063/5.0002337.
18. O. Sugar Gabor, A. Koreanschi, and R. Botez, "A new non-linear vortex lattice method: Applications to wing aerodynamic optimizations," Chinese Journal of Aeronautics, vol. 29, Aug. 2016, doi: 10.1016/j.cja.2016.08.001.
19. H. Goitia and R. Llamas, "Nonlinear vortex lattice method for stall prediction," MATEC Web of Conferences, vol. 304, p. 02006, Jan. 2019, doi: 10.1051/matecconf/201930402006.
20. C. Conlan-Smith, N. Ramos-García, O. Sigmund, and C. S. Andreasen, "Aerodynamic Shape Optimization of Aircraft Wings Using Panel Methods," AIAA Journal, vol. 58, no. 9, pp. 3765–3776, Sep. 2020, doi: 10.2514/1.J058979.
21. I. Lappas and A. Ikenaga, "Conceptual Design and Performance Optimization of a Tip Device for a Regional Turboprop Aircraft," Aerospace, vol. 6, no. 10, Art. no. 10, Oct. 2019, doi: 10.3390/aerospace6100107.
22. M. Segui and R. Botez, "Aerodynamic Coefficients Prediction from Minimum Computa-tion Combinations Using OpenVSP Software," Jan. 2018.
23. A. Hahn, "Open Vehicle Sketch Pad Aircraft Modeling Strategies," in 51st AIAA Aerospace Sciences Meeting including the New Horizons Forum and Aerospace Exposi-tion, American Institute of Aeronautics and Astronautics, 2013. doi: 10.2514/6.2013-331.
24. W. Fredericks et al., "Aircraft Conceptual Design Using Vehicle Sketch Pad," in 48th AIAA Aerospace Sciences Meeting Including the New Horizons Forum and Aerospace Exposition, American Institute of Aeronautics and Astronautics, 2010. doi: 10.2514/6.2010-658.
25. "Parasitedrag [OpenVSP]." http://openvsp.org/wiki/doku.php?id=parasitedrag.
26. O. Gur, W. H. Mason, and J. A. Schetz, "Full-Configuration Drag Estimation," Journal of Aircraft, vol. 47, no. 4, pp. 1356–1367, 2010, doi: 10.2514/1.47557.
27. "(PDF) Subsonic Aircraft Wing Conceptual Design Synthesis and Analysis." https://www.researchgate.net/publication/319325402_Subsonic_Aircraft_Wing_Conceptual_Design_Synthesis_and_Analysis.
28. J. D. Anderson, Introduction to flight, 3rd ed. New York: McGraw-Hill, 1989.
29. M. Parenteau, "Aerodynamic Optimization of Aircraft Wings Using a Coupled VLM-2.5D RANS Approach," p. 104.
30. Z. Lyu, G. K. Kenway, and J. R. R. A. Martins, "RANS-based Aerodynamic Shape Optimization Investigations of the Common Research Model Wing," in 52nd Aerospace Sciences Meeting, American Institute of Aeronautics and Astronautics, 2014. doi: 10.2514/6.2014-0567.

31. P. J. Hoe and N. A. R. N. Mohd, "Numerical Prediction of Blended Wing Body Aerody-namic Characteristics at Subsonic Speed," Jurnal Teknologi, vol. 71, no. 2, Art. no. 2, Nov. 2014, doi: 10.11113/jt.v71.3722.

Notations

kg = kilogram
N = Newton
kW = kilowatt
m = metre
T = temperature
K = Kelvin
p = pressure
kPa = kilopascal
v = velocity
ρ = density
v = kinematic viscosity
Re = Reynolds Number
a = Speed of sound
M = Mach Number
α = Angle of attack
W = Gross take-off weight
b = Wingspan
S_{ref} = Wing reference area
AR = Aspect ratio
c_r = Root chord
c_t = Tip chord
λ = Taper ratio
MAC = Mean aerodynamic chord
S_{wet} = Wetted area
Λ_{LE} = Leading edge sweep
H = Ceiling height
C_L = Coefficient of lift
Cl_{max} = Maximum coefficient of lift
C_{D0} = Parasite drag coefficient
C_{Di} = Induced drag coefficient
C_D = Total drag coefficient
C_p = Coefficient of pressure
C_f = Skin friction coefficient
C_{fe} = Equivalent skin friction coefficient
δ = Boundary layer thickness
δ^*, d^* = Displacement thickness
θ, theta = Momentum thickness
u = flow velocity
u_∞ = free stream velocity
X = chord length in x-direction
∇ = Laplace operator
ϕ = Potential function
$\overrightarrow{V_0}$ = Velocity vector
e = Span efficiency
FF = Form Factor
T_{req} = Thrust Required
P_{req} = Power Required